AIP | Physics of Plasmas

A sharp boundary model for the vertical and kink stability of large aspect-ratio vertically elongated tokamak plasmas

R. Fitzpatrick

Citation: Physics of Plasmas (1994-present) **15**, 092502 (2008); doi: 10.1063/1.2975359
View online: http://dx.doi.org/10.1063/1.2975359
View Table of Contents: http://scitation.aip.org/content/aip/journal/pop/15/9?ver=pdfcov
Published by the AIP Publishing

A sharp boundary model for the vertical and kink stability of large aspect-ratio vertically elongated tokamak plasmas

R. Fitzpatrick
Institute for Fusion Studies, Department of Physics, University of Texas at Austin, Austin, Texas 78712, USA

(Received 3 April 2008; accepted 4 August 2008; published online 2 September 2008)

A relatively straightforward version of the well-known sharp boundary model is developed in order to investigate the ideal $n=0$ and $n=1$ stability of large aspect-ratio, high-β, tokamak plasmas with vertically elongated poloidal cross sections which are surrounded by either ideal, resistive, or partial conducting walls. All calculations made using the model reduce to comparatively simple matrix eigenvalue problems. Various example calculations are described. © *2008 American Institute of Physics*. [DOI: 10.1063/1.2975359]

I. INTRODUCTION

The promising "advanced tokamak" concept is only economically viable provided that the β-limit associated with the $n=1$ ideal "kink" instability is raised substantially in the presence of a close-fitting ideal wall.[1–3] (Here, β is the ratio of the mean energy density of the plasma to that of the magnetic field, and n the toroidal mode number of the instability.) Furthermore, advanced tokamaks invariably employ plasma equilibria whose poloidal cross sections are highly elongated (in the vertical direction). Such elongation has a beneficial effect on both plasma confinement and stability, but is limited by the $n=0$ ideal "vertical" instability.[4] Fortunately, this mode can also be stabilized by a close-fitting ideal wall.[5]

The "sharp-boundary" model of a tokamak plasma, in which all of the equilibrium plasma current is concentrated at the plasma boundary, was first proposed by Freidberg and Haas,[6] and was subsequently elaborated by many researchers (see Ref. 7 and references therein). Within the context of this model, an analytic treatment of ideal $n=0$ and $n=1$ stability yields comparatively simple matrix eigenvalue equations, even when a realistic plasma equilibria (i.e., high-β, strongly elongated, equilibria) are employed. The model is far simpler (but, obviously, less accurate) than a direct numerical simulation.[8–12] On the other hand, it is much more realistic than conventional analytic models which treat the plasma as a low-β periodic cylinder.[13] The advantages of the sharp boundary model, in this respect, were recently pointed out in Ref. 14, where the model was used to analyze the feedback stabilization of the resistive wall mode in large aspect-ratio, high-β, tokamak plasmas with circular poloidal cross sections.

The main limitations of the sharp boundary model are that it cannot deal with high-l_i plasmas (where l_i is the plasma self-inductance), and neglects toroidal coupling (i.e., coupling of different poloidal harmonics due solely to the finite aspect ratio of the plasma). Hence, we would not expect the model to give accurate results for plasmas with strongly peaked current profiles, or with low aspect ratios. On the other hand, the sharp boundary model calculates the plasma eigenfunction in a completely self-consistent manner (i.e., the shape of the plasma eigenfunction at the boundary is not prescribed prior to the calculation), unlike the well-known VALEN code which (in its standard single-mode incarnation) employs an eigenfunction with a prescribed shape at the plasma boundary.[12] The sharp boundary model is superior to the low-β cylindrical model because it deals with pressure gradient driven, rather than current gradient driven, instabilities, and also yields realistic mode eigenfunctions which "balloon" on the outboard side the plasma. (Of course, the cylindrical mode is incapable of distinguishing between the outboard and inboard sides of the plasma.)

In this paper, we employ a version of the sharp boundary model developed by Freidberg and Haas[15] for plasmas with elliptical poloidal cross sections. This model is used to analyze the ideal $n=0$ and $n=1$ stability of large aspect ratio (i.e., $\epsilon \ll 1$, where ϵ is the inverse aspect ratio), high-β (i.e., $\beta \sim \epsilon$), vertically elongated, tokamak plasmas which are surrounded either by ideal walls or by thin resistive walls with poloidally varying electrical resistivity. Our treatment is more general than that of Freidberg and Haas, first because we investigate the stability of the $n=0$ vertical mode, as well as $n>0$ kink modes, and second because we also incorporate resistive walls into the analysis.

II. COORDINATES

Consider a large aspect-ratio, axisymmetric, toroidal plasma equilibrium of major radius R. Let x and z be horizontal and vertical Cartesian coordinates, respectively, in the poloidal plane, which are defined such that the geometric center of the plasma lies at $x=z=0$. Furthermore, let $\mu(x,z)$ be a label for a set of nested axisymmetric toroidal surfaces, and $\nu(x,z)$ an anglelike poloidal coordinate. Suppose that[15]

$$x = a\sqrt{\kappa^2 - 1}\,\sinh\mu\cos\nu, \tag{1}$$

$$z = a\sqrt{\kappa^2 - 1}\,\cosh\mu\sin\nu, \tag{2}$$

where a is the plasma minor radius, and $\kappa \geqslant 1$. It follows that the $\mu=$const surfaces are concentric vertically elongated ellipses. The innermost (zero volume) surface corresponds to $\mu=0$, whereas the outermost (infinite volume) surface corre-

sponds to $\mu=\infty$. Note that $\nabla\mu\cdot\nabla\nu=0$ everywhere in the poloidal plane. It is easily demonstrated that $|\nabla\mu|=|\nabla\nu|=(ah)^{-1}$, where

$$h(\mu,\nu)=\sqrt{\kappa^2-1}(\sinh^2\mu+\cos^2\nu)^{1/2}. \tag{3}$$

Moreover, if ϕ is the toroidal angle, then $|\nabla\phi|=R^{-1}$, assuming that $\epsilon\equiv a/R\ll 1$. A general vector can be written $\mathbf{A}=A_\mu\mathbf{e}_\mu+A_\nu\mathbf{e}_\nu+A_\phi\mathbf{e}_\phi$, where $\mathbf{e}_\mu=\nabla\mu/|\nabla\mu|$, etc. In the following, we employ μ, ν, ϕ as a set of orthogonal curvilinear coordinates.

III. PLASMA EQUILIBRIUM

Let the plasma boundary coincide with the toroidal surface $\mu=\mu_a$, where $\mu_a=\tanh^{-1}(\kappa^{-1})$. This implies that, in the poloidal plane, the plasma is bounded by the vertically elongated ellipse $x=a\cos\nu$, $z=\kappa a\sin\nu$. It follows that the parameter κ represents the plasma vertical elongation.

The central assumption of the sharp boundary model is that the plasma equilibrium is current-free with a constant internal pressure P. It immediately follows that there is zero equilibrium poloidal magnetic field inside the plasma. However, an equilibrium poloidal field is generated outside the plasma by a toroidal sheet current flowing on the boundary.

Let $\mathbf{B}$ and $\hat{\mathbf{B}}$ be the equilibrium magnetic fields inside and outside the plasma, respectively. We can write $B_\phi=B_i/(1+x/R)$ and $\hat{B}_\phi=B_o/(1+x/R)$, where B_i, B_o are constants. On the plasma boundary, $B_\mu=\hat{B}_\mu=B_\nu=0$ and $\hat{B}_\nu=\hat{B}_\nu(\nu)$. Pressure balance across the boundary yields[6]

$$2\mu_0 P+\left(\frac{B_i}{1+\epsilon\cos\nu}\right)^2=\left(\frac{B_o}{1+\epsilon\cos\nu}\right)^2+\hat{B}_\nu^2. \tag{4}$$

It is convenient to adopt the high-β [i.e., $\beta\sim\mathcal{O}(\epsilon)$, rather than $\beta\sim\mathcal{O}(\epsilon^2)$] ordering scheme $\beta\sim\epsilon$, $(B_o-B_i)/B_o\sim\epsilon$, and $\beta+B_i^2/B_o^2-1\sim\epsilon^2$. Here, $\beta=2\mu_0P/B_o^2$. Expansion of Eq. (4) to lowest order in ϵ yields[6,15]

$$\left(\frac{\hat{B}_\nu}{\epsilon B_o}\right)^2=A+2(\beta/\epsilon)\cos\nu+\mathcal{O}(\epsilon), \tag{5}$$

where A is an $\mathcal{O}(1)$ constant.

The safety factor at the plasma boundary takes the form[6,15]

$$q_a=\oint\frac{h_a(\nu)}{\hat{B}_\nu(\nu)/\epsilon B_o}\frac{d\nu}{2\pi}+\mathcal{O}(\epsilon), \tag{6}$$

whereas the toroidal plasma current is written

$$\mu_0 I_\phi=\oint h_a(\nu)\hat{B}_\nu(\nu)d\nu. \tag{7}$$

Here,

$$h_a(\nu)\equiv h(\mu_a,\nu)=[1+(\kappa^2-1)\cos^2\nu]^{1/2}. \tag{8}$$

IV. PERTURBED PLASMA EQUILIBRIUM

Consider a marginally stable, ideal plasma instability. (We can assume that the mode is marginally stable because we are trying to find its stability boundary, rather than its growth rate.) In accordance with the central assumption of the sharp boundary model, the perturbed current and pressure are both zero inside the plasma. Hence, we can write the perturbed magnetic field inside and outside the plasma in the form $\delta\mathbf{B}=\mathrm{i}\nabla V$ and $\delta\hat{\mathbf{B}}=\mathrm{i}\nabla\hat{V}$, respectively, where $\nabla^2V=\nabla^2\hat{V}=0$.

According to Ref. 16, the appropriate matching conditions at the plasma boundary ($\mu=\mu_a$) are

$$\mathbf{e}_\mu\cdot\delta\mathbf{B}=\mathbf{B}\cdot\nabla\xi-\xi\mathbf{e}_\mu\cdot(\mathbf{e}_\mu\cdot\nabla)\mathbf{B}, \tag{9}$$

$$\mathbf{e}_\mu\cdot\delta\hat{\mathbf{B}}=\hat{\mathbf{B}}\cdot\nabla\xi-\xi\mathbf{e}_\mu\cdot(\mathbf{e}_\mu\cdot\nabla)\hat{\mathbf{B}}, \tag{10}$$

$$\mathbf{B}\cdot\delta\mathbf{B}-\hat{\mathbf{B}}\cdot\delta\hat{\mathbf{B}}=-[\xi\mathbf{e}_\mu\cdot\nabla(B^2/2)-\xi\mathbf{e}_\mu\cdot\nabla(\hat{B}^2/2)], \tag{11}$$

where $\xi(\nu,\phi)$ is the normal plasma displacement. The first two conditions ensure that the perturbed plasma boundary remains a magnetic flux surface, whereas the final condition ensures that it remains in pressure balance.

It is easily demonstrated that, to lowest order in ϵ,

$$\mathbf{e}_\mu\cdot\delta\mathbf{B}=\mathrm{i}(ah_a)^{-1}\frac{\partial V}{\partial\mu}, \tag{12}$$

$$\mathbf{e}_\mu\cdot\delta\hat{\mathbf{B}}=\mathrm{i}(ah_a)^{-1}\frac{\partial\hat{V}}{\partial\mu}, \tag{13}$$

$$\mathbf{B}\cdot\nabla\xi\simeq\frac{B_o}{R}\frac{\partial\xi}{\partial\phi}, \tag{14}$$

$$\hat{\mathbf{B}}\cdot\nabla\xi\simeq\left(\frac{\hat{B}_\nu}{ah_a}\frac{\partial}{\partial\nu}+\frac{B_o}{R}\frac{\partial}{\partial\phi}\right)\xi, \tag{15}$$

$$\mathbf{e}_\mu\cdot(\mathbf{e}_\mu\cdot\nabla)\mathbf{B}=0, \tag{16}$$

$$\mathbf{e}_\mu\cdot(\mathbf{e}_\mu\cdot\nabla)\hat{\mathbf{B}}=-\frac{1}{ah_a}\frac{\partial\hat{B}_\nu}{\partial\nu}, \tag{17}$$

$$\mathbf{B}\cdot\delta\mathbf{B}\simeq\mathrm{i}\frac{B_o}{R}\frac{\partial V}{\partial\phi}, \tag{18}$$

$$\hat{\mathbf{B}}\cdot\delta\hat{\mathbf{B}}\simeq\mathrm{i}\left(\frac{\hat{B}_\nu}{ah_a}\frac{\partial}{\partial\nu}+\frac{B_o}{R}\frac{\partial}{\partial\phi}\right)\hat{V}, \tag{19}$$

$$\mathbf{e}_\mu\cdot\nabla(B^2/2)\simeq-\frac{\kappa}{h_a}\frac{B_i^2}{R}\cos\nu, \tag{20}$$

$$\mathbf{e}_\mu\cdot\nabla(\hat{B}^2/2)\simeq-\frac{\kappa}{h_a}\left(\frac{\hat{B}_\nu^2}{ah_a^2}+\frac{B_o^2}{R}\cos\nu\right). \tag{21}$$

Thus, the matching conditions at the plasma boundary reduce to

$$\mathrm{i}\frac{\partial V}{\partial\mu}=\epsilon B_o h_a\frac{\partial\xi}{\partial\phi}, \tag{22}$$

$$\mathrm{i}\frac{\partial \hat{V}}{\partial \mu} = \left(\hat{B}_\nu \frac{\partial}{\partial \nu} + \epsilon B_o h_a \frac{\partial}{\partial \phi}\right)\xi + \frac{\partial \hat{B}_\nu}{\partial \nu}\xi, \tag{23}$$

$$\mathrm{i}\left(\hat{B}_\nu \frac{\partial}{\partial \nu} + \epsilon B_o h_a \frac{\partial}{\partial \phi}\right)\hat{V} - \mathrm{i}\epsilon B_o h_a \frac{\partial V}{\partial \phi} = \kappa\left(\frac{\hat{B}_\nu^2}{h_a^2} + \epsilon B_o^2 \beta \cos\nu\right)\xi. \tag{24}$$

V. NORMALIZATION

It is convenient to normalize V, $\hat{V}$ to $a\epsilon B_o$, ξ to a, $\hat{B}_\nu$ to ϵB_o, and I_ϕ to $a\epsilon B_o/\mu_0$. Using this normalization scheme, the plasma equilibrium is described by the following set of equations:[15]

$$\alpha Q(\alpha) = \pi q_a \hat{\beta}^{1/2}, \tag{25}$$

$$Q(\alpha) = \frac{1}{2}\int_0^\pi \frac{h_a(\nu)d\nu}{[1-\alpha^2\sin^2(\nu/2)]^{1/2}}, \tag{26}$$

$$A = 2\hat{\beta}\left(\frac{2}{\alpha^2} - 1\right), \tag{27}$$

$$\hat{B}_\nu = (A + 2\hat{\beta}\cos\nu)^{1/2}, \tag{28}$$

$$I_\phi = 2\int_0^\pi h_a(\nu)\hat{B}_\nu(\nu)d\nu, \tag{29}$$

where $\hat{\beta}=\beta/\epsilon$. Note that, at fixed β, $q_a\to\infty$ as $\alpha\to 1$, whereas I_ϕ remains finite. This is a consequence of a slight peculiarity of sharp boundary equilibria.[6] Namely, at fixed β, there is a minimum plasma current required to maintain the equilibrium, irrespective of the value of the edge-q.

The normalized matching conditions at the plasma boundary are

$$\mathrm{i}\frac{\partial V}{\partial \mu} = h_a \frac{\partial \xi}{\partial \phi}, \tag{30}$$

$$\mathrm{i}\frac{\partial \hat{V}}{\partial \mu} = \left(\hat{B}_\nu \frac{\partial}{\partial \nu} + h_a \frac{\partial}{\partial \phi}\right)\xi + \frac{\partial \hat{B}_\nu}{\partial \nu}\xi, \tag{31}$$

$$\mathrm{i}\left(\hat{B}_\nu \frac{\partial}{\partial \nu} + h_a \frac{\partial}{\partial \phi}\right)\hat{V} - \mathrm{i}h_a \frac{\partial V}{\partial \phi} = \kappa\left(\frac{\hat{B}_\nu^2}{h_a^2} + \hat{\beta}\cos\nu\right)\xi. \tag{32}$$

Finally, the potentials V and $\hat{V}$ satisfy

$$\frac{\partial^2 V}{\partial^2 \mu} + \frac{\partial^2 V}{\partial^2 \nu} \simeq 0, \tag{33}$$

$$\frac{\partial^2 \hat{V}}{\partial^2 \mu} + \frac{\partial^2 \hat{V}}{\partial^2 \nu} \simeq 0. \tag{34}$$

VI. BOUNDARY CONDITIONS

Suppose that all perturbed quantities vary toroidally as $\exp(-\mathrm{i}n\phi)$, where n is the toroidal mode number.

Now, in order to ensure that the perturbed magnetic field is *finite* and continuous at the center of the plasma (i.e., $\mu\to 0$), the potential $V(\mu,\nu,\phi)$ must satisfy the boundary conditions

$$V(0,\nu,\phi) = V(0,\pi-\nu,\phi), \tag{35}$$

$$\frac{\partial V}{\partial \mu}(0,\nu,\phi) = -\frac{\partial V}{\partial \mu}(0,\pi-\nu,\phi). \tag{36}$$

This follows because the $\mu=0$ surface corresponds to the zero minor radius ellipse $x=0$, $y=\sin\nu$. The most general solution of Eq. (33) which is consistent with the above constraints is[15]

$$V(\mu,\nu,\phi) = \sum_m \{a_m \cosh(m\mu)\cos[m(\nu-\pi/2)] + b_m \sinh(m\mu)\sin[m(\nu-\pi/2)]\}\mathrm{e}^{-\mathrm{i}n\phi}, \tag{37}$$

where the a_m and b_m are constants.

Assuming the existence of an ideal wall which coincides with the toroidal surface $\mu=\mu_w$ (where $\mu_w>\mu_a$), the potential $\hat{V}$ satisfies the boundary condition

$$\left(\frac{\partial \hat{V}}{\partial \mu}\right)_{\mu=\mu_w} = 0. \tag{38}$$

The most general solution of Eq. (34) which is consistent with this constraint is

$$\hat{V}(\mu,\nu,\phi) = \sum_m \hat{a}_m \cosh[m(\mu-\mu_w)]\mathrm{e}^{\mathrm{i}(m\nu-n\phi)}, \tag{39}$$

where the $\hat{a}_m$ are constants.

It should be noted that the wall does not, in general, lie on an equilibrium magnetic flux surface. However, this is not a problem because real walls are resistive in nature, and only act as ideal conductors on time scales significantly shorter than their characteristic L/R times. In modern-day tokamaks, the lifetime of the discharge is always much longer than the L/R time of the wall, while the inverse growth rate of an ideal plasma instability is always very much shorter than this time. Hence, the wall generally has no influence on the plasma equilibrium, but acts as a perfect conductor as far as ideal instabilities are concerned. In particular, the equilibrium magnetic field has sufficient time to fully penetrate the wall, and so there is no requirement that the wall should lie on an equilibrium magnetic flux surface.

VII. IDEAL STABILITY

Let

$$\xi(\nu,\phi) = \sum_{m\neq 0} \xi_m \mathrm{e}^{\mathrm{i}(m\nu-n\phi)}, \tag{40}$$

where the ξ_m are constants.

The first matching condition [Eq.(30)] yields

$$\sum_m \{a_m m \sinh(m\mu_a)\cos[m(\nu-\pi/2)] + b_m m \cosh(m\mu_a)\sin[m(\nu-\pi/2)]\} = \sum_{m,m'} e^{im\nu} G_{mm'}\xi_{m'}, \tag{41}$$

where

$$G_{mm'} = -\int_0^\pi n h_a(\nu)\cos[(m'-m)\nu]\frac{d\nu}{\pi}. \tag{42}$$

It follows that

$$a_m = \frac{e^{im\pi/2}}{m\sinh(m\mu_a)}\sum_{m'} G_{mm'}\xi_{m'}, \tag{43}$$

$$b_m = \frac{ie^{im\pi/2}}{m\cosh(m\mu_a)}\sum_{m'} G_{mm'}\xi_{m'}. \tag{44}$$

Note that a_0 and b_0 are singular unless[15]

$$\sum_m G_{0m'}\xi_{m'} = 0. \tag{45}$$

The above constraint ensures that the plasma perturbation is incompressible, and therefore maximally unstable, and allows us to set $a_0=b_0=0$ without loss of generality. Hence, from Eq. (37) and Eqs. (43)–(45),

$$V(\mu_a,\nu,\phi) = \sum_{m\neq 0} e^{i(m\nu-n\phi)}|m|^{-1} \times\left[\frac{1+\zeta^{2|m|}}{1-\zeta^{2|m|}}G_{mm'} + \frac{2(-\zeta)^{|m|}}{1-\zeta^{2|m|}}G_{-mm'}\right]\xi_{m'}, \tag{46}$$

$$\frac{\partial V}{\partial\mu}(\mu_a,\nu,\phi) = \sum_{m\neq 0} e^{i(m\nu-n\phi)} G_{mm'}\xi_{m'}, \tag{47}$$

where $\zeta=(\kappa-1)/(\kappa+1)$.

The second matching condition [Eq. (31)] gives

$$\sum_m \hat{a}_m m \sinh[m(\mu_a-\mu_w)]e^{im\nu} = \sum_{m,m'} e^{im\nu}\hat{G}_{mm'}\xi_{m'}, \tag{48}$$

where

$$\hat{G}_{mm'} = \int_0^\pi [m\hat{B}_\nu(\nu) - n h_a(\nu)]\cos[(m'-m)\nu]\frac{d\nu}{\pi}. \tag{49}$$

It follows that

$$\hat{a}_m = \frac{1}{m\sinh[m(\mu_a-\mu_w)]}. \tag{50}$$

Again, the constraint (45) allows us to set $\hat{a}_m=0$ (note that $\hat{G}_{0m}=G_{0m}$). Hence, from Eqs. (39) and (50), we obtain

$$\hat{V}(\mu_a,\nu,\phi) = -\sum_{m\neq 0} e^{i(m\nu-n\phi)}|m|^{-1}\left(\frac{1+r_w^{-2|m|}}{1-r_w^{-2|m|}}\right)\hat{G}_{mm'}\xi_{m'}, \tag{51}$$

$$\frac{\partial\hat{V}}{\partial\mu}(\mu_a,\nu,\phi) = \sum_{m\neq 0} e^{i(m\nu-n\phi)}\hat{G}_{mm'}\xi_{m'}, \tag{52}$$

where $r_w\equiv\exp(\mu_w-\mu_a)$ is approximately the ratio of the minor radius of the wall to that of the plasma.

The final matching condition [Eq. (32)] can be combined with Eqs. (46) and (51) to give

$$\sum_{m'} F_{mm'}\xi_{m'} = 0, \tag{53}$$

where[15]

$$F_{mm'} = \sum_{k\neq 0} G_{km}|k|^{-1}\left[\frac{1+\zeta^{2|k|}}{1-\zeta^{2|k|}}G_{km'} + \frac{2(-\zeta)^{|k|}}{1-\zeta^{2|k|}}G_{-km'}\right] + \sum_{k\neq 0}\hat{G}_{km}|k|^{-1}[(1+r_w^{-2|k|})/(1-r_w^{-2|k|})]\hat{G}_{km'} - H_{mm'}, \tag{54}$$

and

$$H_{mm'} = \kappa\int_0^\pi\left(\frac{\hat{B}_\nu^2}{h_a^2} + \hat{\beta}\cos\nu\right)\cos[(m'-m)\nu]d\nu. \tag{55}$$

Observe that the so-called force matrix $F_{mm'}$ is real and symmetric.

The stability problem reduces to the solution of the eigenmode equation

$$\sum_{m'} F_{mm'}\xi_{m'} = \lambda\xi_m, \tag{56}$$

subject to the constraint $\Sigma_{m'}G_{0m'}\xi_{m'}=0$. (Of course, only the $\lambda=0$ solution, which corresponds to the marginal stable case, is physical.) This is equivalent to solving the unconstrained eigenmode equation[15]

$$\sum_{m'} \tilde{F}_{mm'}z_{m'} = \lambda z_m, \tag{57}$$

where $\tilde{F}_{mm'}=\Sigma_{k,l}P_{mk}F_{kl}P_{lm'}$, and

$$P_{mm'} = \delta_{mm'} - \frac{G_{0m}G_{0m'}}{\Sigma_k G_{0k}^2}, \tag{58}$$

with $\xi_m=\Sigma_{m'}P_{mm'}z_{m'}$. Note that the $\tilde{F}_{mm'}$ matrix is real and symmetric, which guarantees that all of its eigenvalues are real. According to the ideal energy principle, the plasma is ideally unstable if any of the eigenvalues of Eq. (57) are negative, and stable otherwise.[16]

The $n=0$ mode is a special case, since the constraint (45) is automatically satisfied due to the fact that the $G_{0m'}$ are all zero. In this situation, the plasma perturbation can be made incompressible by simply setting $\xi_0=0$. Hence, the eigenmode equation for the $n=0$ mode is

$$\sum_{m'\neq 0} F_{mm'}\xi_{m'} = \lambda\xi_m \tag{59}$$

for $m\neq 0$.

VIII. RESISTIVE WALL MODE STABILITY

Suppose that, instead of being ideal, the wall surrounding the plasma is thin and resistive. Let the inner and outer boundaries of the wall lie on the toroidal surfaces $\mu=\mu_w$ and $\mu=\mu_w+\delta\mu_w$, respectively, where $0<\delta\mu_w\ll\mu_w$. Furthermore, let the wall electrical conductivity be $\sigma_w(\nu)$. In the following, we shall examine the stability of the so-called resistive wall mode,[17] which grows on the L/R time of the wall.

The Ampère–Maxwell equation gives $\nabla\times\delta\hat{\mathbf{B}}=\mu_0\mathbf{j}$, where $\mathbf{j}$ is the current density in the wall. Taking the ϕ component of this equation, and integrating (in μ) across the wall, we obtain

$$\int_{\mu_w}^{\mu_w+\delta\mu_w} a^{-1}h^{-2}\left[\frac{\partial(h\delta\hat{B}_\nu)}{\partial\mu}-\frac{\partial(h\delta\hat{B}_\mu)}{\partial\nu}\right]d\mu=\mu_0 J_\phi, \tag{60}$$

where,

$$J_\phi(\nu,\phi)=\int_{\mu_w}^{\mu_w+\delta\mu_w} j_\phi d\mu. \tag{61}$$

In the limit in which the wall thickness is negligible, the above equation reduces to

$$\mu_0 J_\phi=(ah_w)^{-1}[\delta\hat{B}_\nu]_{\mu_w}^{\mu_w+\delta\mu_w}, \tag{62}$$

where $h_w(\nu)\equiv h(\mu_w,\nu)$.

Inside the wall, the μ component of the curl of Ohm's law gives $-\gamma\delta\hat{B}_\mu=\mathbf{e}_\mu\cdot\nabla\times(\sigma_w^{-1}\mathbf{j})$, where γ is the mode growth rate. This equation yields

$$-\gamma\delta\hat{B}_\mu=a^{-1}\left[h_w^{-1}\frac{\partial(\sigma_w^{-1}j_\phi)}{\partial\nu}-\epsilon\frac{\partial(\sigma_w^{-1}j_\nu)}{\partial\phi}\right]. \tag{63}$$

Now, it is easily demonstrated that $j_\nu\sim\epsilon j_\phi$. Hence, the second term on the right-hand side of the above equation can be neglected. Integrating (in μ) across the wall, and making use of the well-known "thin-shell approximation" (which basically involves neglecting the μ variation of $\delta\hat{B}_\mu$ across the wall[16]), we obtain

$$-\mu_0\gamma\delta\mu_w\delta\hat{B}_\mu|_{\mu_w}=(ah_w)^{-1}\frac{\partial}{\partial\nu}\{(\sigma_w ah_w)^{-1}[\delta\hat{B}_\nu]_{\mu_w}^{\mu_w+\delta\mu_w}\}, \tag{64}$$

where use has been made of Eq. (62). Finally, since $\delta\hat{\mathbf{B}}=\mathrm{i}\nabla\hat{V}$, the boundary condition at the wall becomes

$$\left.\frac{\partial\hat{V}}{\partial\mu}\right|_{\mu_w}=-\frac{\partial}{\partial\nu}\left(\lambda^{-1}\left[\frac{\partial\hat{V}}{\partial\nu}\right]_{\mu_w}^{\mu_w+\delta\mu_w}\right), \tag{65}$$

where $\lambda(\nu)=\gamma\mu_0 a^2\delta\mu_w\sigma_w(\nu)h_w^2(\nu)$.

In the vacuum region inside the wall, we can write

$$\hat{V}(\mu,\nu)=\sum_{m\neq0}[\hat{a}_m\mathrm{e}^{-|m|(\mu-\mu_w)}+\hat{b}_m\mathrm{e}^{|m|(\mu-\mu_w)}]\mathrm{e}^{\mathrm{i}m\nu}, \tag{66}$$

where $\hat{a}_m$ and $\hat{b}_m$ are constants, and we have neglected the common $\exp(-\mathrm{i}n\phi)$ dependence of perturbed quantities, for the sake of simplicity. The solution outside the wall which is well-behaved as $\mu\to\infty$, and satisfies the boundary condition that $\delta\hat{B}_\mu$ be continuous across the wall, is

$$\hat{V}(\mu,\nu)=\sum_{m\neq0}[\hat{a}_m\mathrm{e}^{-|m|(\mu-\mu_w)}-\hat{b}_m\mathrm{e}^{-|m|(\mu-\mu_w)}]\mathrm{e}^{\mathrm{i}m\nu}. \tag{67}$$

It follows from Eq. (65) that

$$2\sum_{m\neq0}m\hat{b}_m\mathrm{e}^{\mathrm{i}m\nu}=-\lambda\sum_{m\neq0}\mathrm{sgn}(m)(-\hat{a}_m+\hat{b}_m)\mathrm{e}^{\mathrm{i}m\nu}. \tag{68}$$

Hence, we obtain

$$2m\hat{b}_m=-\sum_{m'\neq0}J_{mm'}\,\mathrm{sgn}(m')(-\hat{a}_{m'}+\hat{b}_{m'}), \tag{69}$$

where

$$J_{mm'}=\oint\lambda(\nu)\cos[(m'-m)\nu]\frac{d\nu}{2\pi}. \tag{70}$$

Note that, for the sake of simplicity, we have assumed that $\lambda(-\nu)=\lambda(\nu)$.

According to the above analysis, in the presence of a thin resistive wall, Eq. (51) generalizes to give

$$\hat{V}(\mu_a,\nu,\phi)=-\sum_{m\neq0,k\neq0}\mathrm{e}^{\mathrm{i}(m\nu-n\phi)}K_{mk}\hat{G}_{km'}\xi_{m'}, \tag{71}$$

where the vacuum matrix $K_{mm'}$ is specified by $\Sigma_{k\neq0}L_{mk}K_{km'}=M_{mm'}$ (for $m,m'\neq0$), with

$$L_{mm'}=2mr_w^{|m|}\delta_{mm'}+J_{mm'}\,\mathrm{sgn}(m')(r_w^{|m'|}-r_w^{-|m'|}), \tag{72}$$

$$M_{mm'}=2\,\mathrm{sgn}(m)r_w^{|m|}\delta_{mm'}+J_{mm'}m'^{-1}(r_w^{|m'|}+r_w^{-|m'|}). \tag{73}$$

Thus, the expression (54) for the force matrix generalizes to

$$F_{mm'}=\sum_{k\neq0}G_{km}|k|^{-1}\left[\frac{1+\zeta^{2|k|}}{1-\zeta^{2|k|}}G_{km'}+\frac{2(-\zeta)^{|k|}}{1-\zeta^{2|k|}}G_{-km'}\right]+\sum_{k\neq0,l\neq0}\hat{G}_{km}K_{kl}\hat{G}_{lm'}-H_{mm'}. \tag{74}$$

The $n>0$ resistive wall mode stability problem is written

$$\sum_{m'}\tilde{F}_{mm'}(\gamma)z_{m'}=0, \tag{75}$$

where $\tilde{F}_{mm'}=\Sigma_{k,l}P_{mk}F_{kl}P_{lm'}$, $\xi_m=\Sigma_{m'}P_{mm'}z_{m'}$, and the $P_{mm'}$ matrix is defined in Eq. (58). The above equation is solved by searching for the largest value of γ which sets the determinant of the $\tilde{F}_{mm'}$ matrix to zero. Now, it is easily demonstrated that the vacuum matrix $K_{mm'}$ is real and symmetric. It follows that the $\tilde{F}_{mm'}$ matrix is also real and symmetric. This ensures that the growth rate γ of the resistive wall mode is real; i.e., the mode always grows or decays without oscillation. Hence, solving Eq. (75) only involves a one-dimensional search along the real axis in γ-space. The $n=0$ resistive wall mode stability problem takes the form

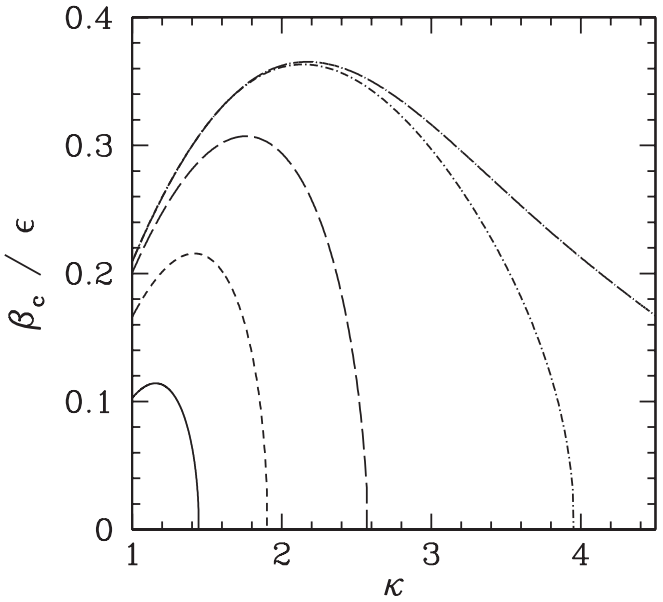

FIG. 1. β-limit for ideal $n=1$ stability vs κ for plasma equilibria with $r_w=10.0$. The solid, short-dashed, long-dashed, dot-short-dashed, and dot-long-dashed curves correspond to $q_a=1.25$, 1.5, 2.0, 4.0, and 8.0, respectively. The stable region lies below the curves.

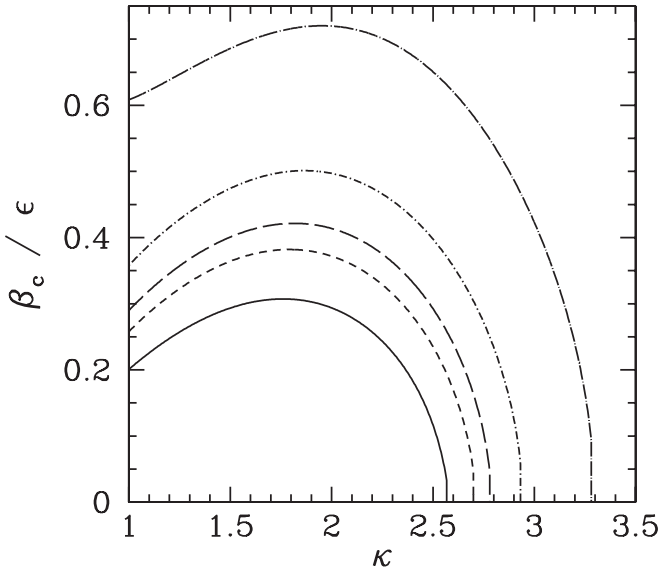

FIG. 2. β-limit for ideal $n=1$ stability vs κ for plasma equilibria with $q_a=2.0$. The solid, short-dashed, long-dashed, and dot-short-dashed, and dot-long-dashed curves correspond to $r_w=10.0$, 1.6, 1.5, 1.4, and 1.3, respectively. The stable region lies below the curves.

$$\sum_{m' \neq 0} F_{mm'}(\gamma)\xi_{m'} = 0 \tag{76}$$

for $m \neq 0$. The solution to the problem proceeds in an analogous manner to the $n>0$ case.

Suppose, finally, that the wall is partial. In other words, let the wall have the uniform conductivity σ_w, but only be present in the angular range $\nu_2 > |\nu| > \nu_1$, where $\pi \geqslant \nu_2 > \nu > \nu_1 \geqslant 0$ (i.e., let $\sigma_w=0$ outside this range). This implies that the wall matrix $J_{mm'}$ takes the form

$$J_{mm'} = \gamma\tau_w \int_{\nu_1}^{\nu_2} h_w^2(\nu)\cos[(m-m')\nu]\frac{d\nu}{\pi}, \tag{77}$$

where $\tau_w=\mu_0 a^2 \delta\mu_w\sigma_w$ is the wall's characteristic L/R time.

IX. NUMERICAL RESULTS

Figure 1 shows the β-limit for the ideal $n=1$ mode as a function of the plasma elongation κ. Calculations are performed for free-boundary plasmas (i.e., $r_w \gg 1$) with various different values of the edge-q. The stable region lies below the curves. It can be seen that plasma elongation is initially stabilizing (i.e., as κ increases above unity there is an initial increase in the β-limit), but that there is a critical value of the elongation beyond which the $n=1$ mode becomes unstable for all (positive) values of β. Note that the region of stability in κ-β space shrinks to zero as $q_a \rightarrow 1$, indicating that the $n=1$ mode is universally unstable for $q_a < 1$. Finally, the stable region increases in area, eventually asymptoting to some fixed limit, as $q_a \rightarrow \infty$. Indeed, as $q_a \rightarrow \infty$, the maximum β-limit, $\beta/\epsilon \sim 0.37$, is obtained when $\kappa \sim 2.2$. All of these conclusions are in accordance with the previously published results of Friedberg and Haas.[15]

Figure 2 shows the β-limit for the ideal $n=1$ mode as a function of the plasma elongation κ. Calculations are performed for plasma equilibria characterized by $q_a=2$ and various different values of the wall radius r_w. It can be seen that the presence of a close-fitting (i.e., $r_w < 1.5$) ideal wall has a significant stabilizing effect on the $n=1$ mode. Indeed, the region of stability becomes infinite in extent in κ-β space as $r_w \rightarrow 1$, indicating that the $n=1$ is universally stable when there is no vacuum gap between the wall and the plasma boundary. This result is well known.[16]

Figure 3 shows a typical $n=1$ ideal eigenfunction. It can be seen that the mode amplitude is much larger on the outboard side of the plasma (i.e., $|\nu| < \pi/2$) than on the inboard

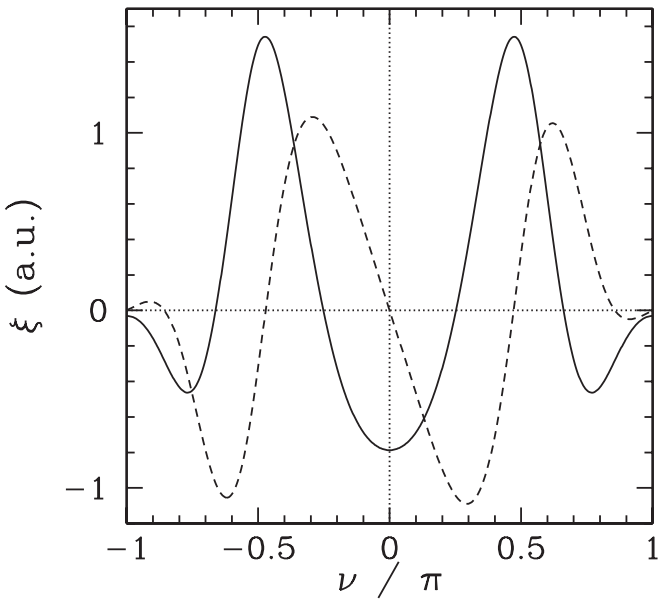

FIG. 3. $n=1$ ideal eigenfunctions $\xi(\nu,0)$ and $\xi(\nu,\pi/2)$, calculated for $q_a=2.0$, $\beta/\epsilon=0.3$, $\kappa=2.0$, and $r_w=10.0$.

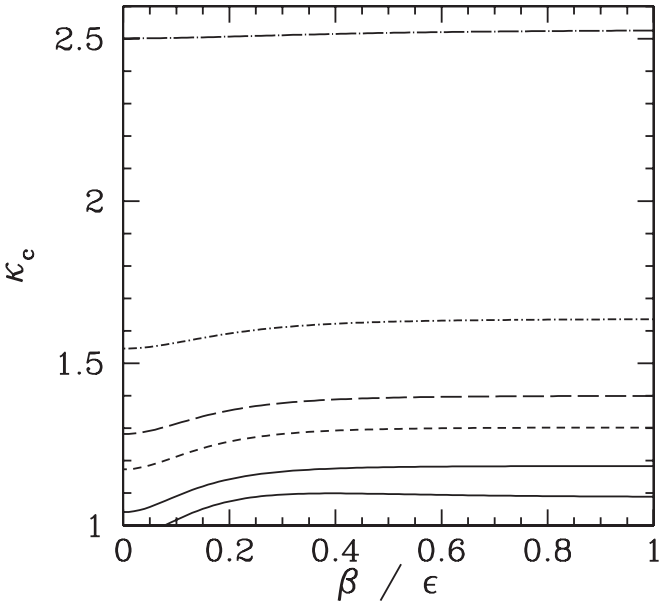

FIG. 4. κ-limit for ideal $n=0$ stability vs β/ϵ for plasma equilibria with $q_a=2.0$. The solid, short-dashed, long-dashed, dot-short-dashed, and dot-long-dashed curves correspond to $r_w=10.0$, 5.0, 4.0, 3.0, and 2.0, respectively. In the case in which there are two stability curves, the stable region lies between the curves. Otherwise, the stable region lies below the curves.

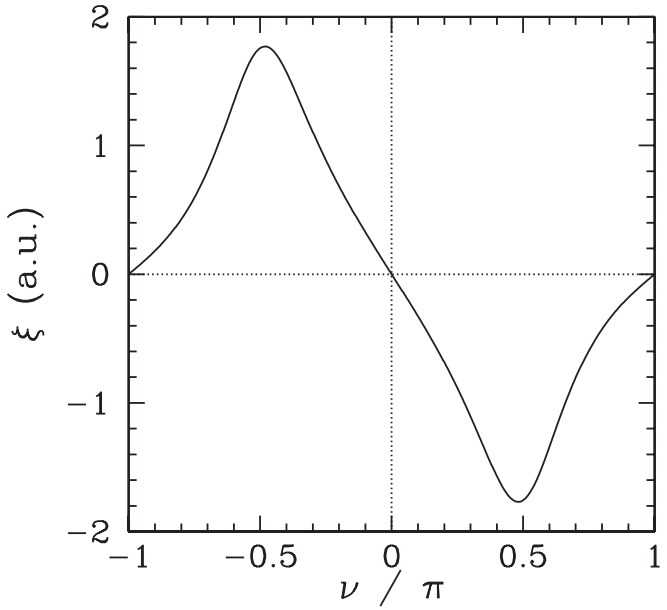

FIG. 5. $n=0$ ideal eigenfunction $\xi(\nu,\pi/2)$, calculated for $q_a=2.0$, $\beta/\epsilon=0.2$, $\kappa=2.0$, and $r_w=10.0$.

side. This "ballooning" of the mode on the outboard midplane is characteristic of a pressure-driven kink-mode.[16]

Figure 4 shows the elongation limit for the ideal $n=0$ mode versus β/ϵ for plasmas with various values of r_w. (Note that, since $n=0$ stability boundaries are found to exhibit very little variation with the edge-q, all of our calculations can be performed using $q_a=2$ with very little loss in generality.) It is clear that, in the presence of a very remote wall (i.e., $r_w=10.0$), the $n=0$ mode is driven unstable by fairly small values of the plasma elongation (i.e., $\kappa>1.1$). However, as the wall is moved closer to the plasma, the mode rapidly becomes much more stable. Indeed, by the time $r_w=2.0$—which still corresponds to a fairly remote wall—the $n=0$ mode can only be driven unstable by comparatively large values of the plasma elongation (i.e., $\kappa>2.5$). We conclude that the $n=0$ "vertical" instability is very easily stabilized by the presence of a close-fitting ideal wall. (Note that the degree of stabilization is much greater than that exhibited in Fig. 2 for the $n=1$ mode.)

Figure 5 shows a typical $n=0$ ideal eigenfunction, verifying that the mode is indeed a vertical instability.

Figure 6 shows the growth rate of the $n=1$ resistive wall mode as a function of β/ϵ, calculated for a realistically shaped plasma equilibrium surrounded by various partial resistive walls. In these calculations, the walls contain a toroidal gap centered on the inboard midplane (i.e., $\nu_1=0$, $\nu_2=f\pi$). Cases are shown for various values of the fractional wall coverage f. Now, we expect the resistive wall mode to become unstable as soon as the ideal kink mode becomes unstable in the absence of a wall.[17] This stability limit is known as the no-wall limit. Is clear, from Fig. 5, that the no-wall β-limit is independent of the degree of wall coverage. This is as expected, since a no-wall stability limit obviously cannot depend on the properties of an absent wall. We also expect the growth rate of the resistive wall mode to tend to infinity as we approach the limit in which the ideal kink mode becomes unstable in the presence of an ideal wall. This stability limit is known as the perfect-wall limit. It can be seen, from Fig. 5, that the perfect-wall β-limit does depend on the degree of wall coverage, becoming smaller as the coverage is reduced. This, again, is as expected.

Figure 7 shows the typical variation of the perfect-wall β-limit for the $n=1$ kink instability with the degree of wall

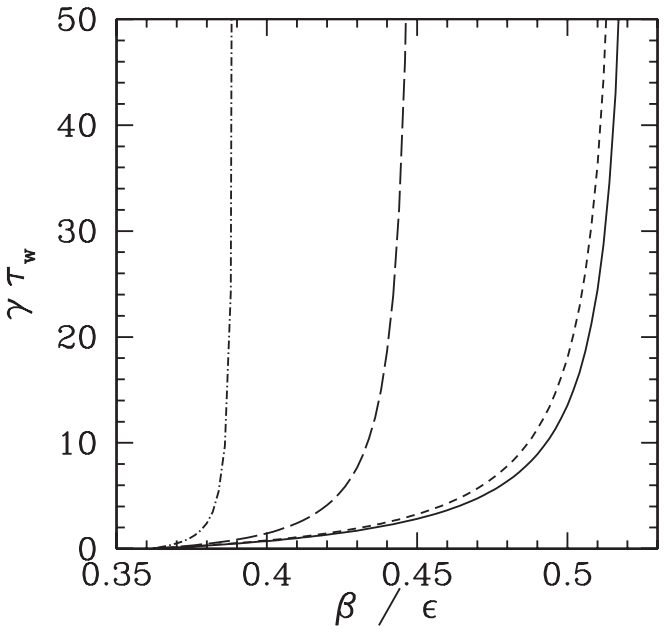

FIG. 6. Growth rate of the $n=1$ resistive wall mode as a function of β/ϵ, calculated for $q_a=4.0$, $\kappa=2.0$, and $r_w=1.4$. The solid, short-dashed, long-dashed, and dot-dashed curves correspond to $f=1.0$, 0.75, 0.50, and 0.25, respectively.

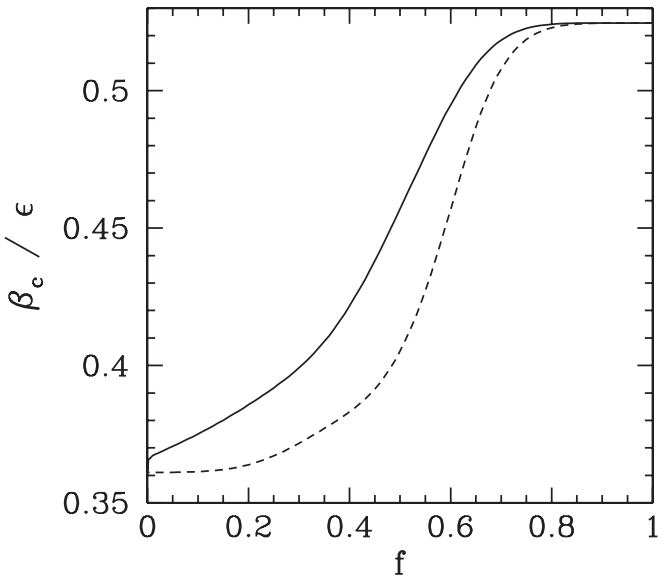

FIG. 7. Perfect-wall β-limit for the $n=1$ kink stability as a function of fractional wall coverage f, calculated for $q_a=4.0$, $\kappa=2.0$, and $r_w=1.4$. The solid and dashed curves correspond to the cases where the gap in the wall is centered on the inboard and outboard midplanes, respectively. The stable region lies below the curves.

coverage. Two cases are shown: the first where the toroidal gap in the wall is centered on the inboard midplane (i.e., $\nu_1=0$, $\nu_2=\pi f$), and the second where the gap is centered on the outboard midplane [i.e., $\nu_1=(1-f)\pi$, $\nu_2=\pi$]. It can be seen that, in both cases, it is possible to remove approximately 20% of the wall without appreciably affecting the β-limit. On the other hand, removal of more than 20% of the wall causes a degradation in the β-limit. Observe that the difference between having the gap on the outboard and the inboard mid-planes is largest when the degree of wall coverage is small. In this situation, a wall segment centered on the outboard midplane has a significantly greater stabilizing effect on the $n=1$ mode than one centered on the inboard midplane. This is, of course, a manifestation of the fact that the $n=1$ eigenfunction balloons on the outboard side of the plasma (see Fig. 3).

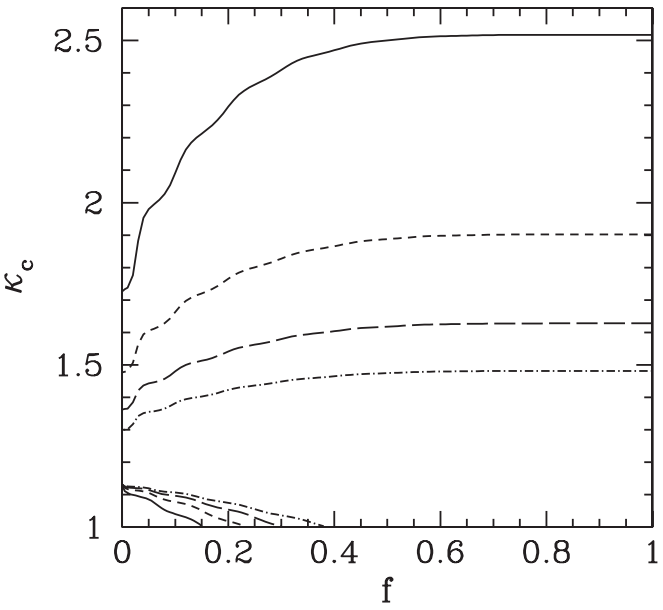

FIG. 8. Perfect-wall κ-limit for $n=0$ vertical stability as a function of fractional wall coverage f, calculated for $q_a=2.0$, and $\beta/\epsilon=0.5$. The solid, short-dashed, long-dashed, and dot-dashed curves correspond to $r_w=2.0$, 2.5, 3.0, and 3.5, respectively. The stable region lies between the upper and lower curves.

Finally, Fig. 8 shows the typical variation of the perfect-wall elongation limit for the $n=0$ vertical instability with the degree of wall coverage. In this calculation, the wall consists of two segments: one directly above the plasma and one directly below [i.e., $\nu_1=(1-f)\pi/2$, $\nu_2=(1+f)\pi/2$]. Cases are shown for various different wall positions. It can be seen that a relatively distant wall (i.e., $r_w=2.0$) is capable of stabilizing the vertical instability, even when up to 60% of the wall is removed (at the inboard and outboard midplanes). However, the ability of the wall to stabilize the mode is significantly degraded if more than 60% of it is removed, or if it is moved further away from the plasma.

X. SUMMARY

A simple, but useful, version of the well-known sharp boundary model has been developed in order to study the $n=0$ and $n=1$ stability of large aspect-ratio, high-β tokamak plasmas with vertically elongated poloidal cross sections which are surrounded by either ideal, resistive, or partial conducting walls. Our model can be regarded as a version of the classic model of Freidberg and Haas[15] which has been extended to deal with $n=0$ modes, resistive walls, and partial walls. Alternatively, it can be thought of as a version of the recently published model of Jhang[14] which has been upgraded to take $n=0$ modes and plasma elongation into account. Within the context of our model, all calculations reduce to comparatively simple matrix eigenvalue problems. Although the model is not as accurate as a direct numerical simulation, it is far simpler to formulate, and much less time-consuming to use, and is therefore ideal for scoping studies of the effect of plasma elongation and different wall configurations on $n=0$ and $n=1$ stability. Moreover, the model is far more realistic than a conventional analytic model which treats the plasma as a low-β periodic cylinder, since it is capable of distinguishing between the inboard and outboard sides of the plasma.

ACKNOWLEDGMENTS

This research was funded by the U.S. Department of Energy under Contract No. DE-FG05-96ER-54346.

[1] F. Troyon, R. Gruber, H. Saurenmann, S. Semenzato, and S. Succi, Plasma Phys. Controlled Fusion **26**, 209 (1984).
[2] C. Kessel, J. Manickam, G. Rewoldt, and W. M. Tang, Phys. Rev. Lett. **72**, 1212 (1994).
[3] E. A. Lazarus, G. A. Navratil, C. M. Greenfield, E. J. Strait, M. E. Austin, K. H. Burrell, T. A. Casper, D. R. Baker, J. C. DeBoo, E. J. Doyle, R. Durst, J. R. Ferron, C. B. Forest, P. Gohil, R. J. Groebner, W. W. Heidbrink, R.-M. Hong, W. A. Houlberg, A. W. Howald, C.-L. Hsieh, A. W. Hyatt, G. L. Jackson, J. Kim, L. L. Lao, C. J. Lasnier, A. W. Leonard, J. Lohr, R. J. La Haye, R. Maingi, R. L. Miller, M. Murakami, T. H. Osborne, L. J. Perkins, C. C. Petty, C. L. Rettig, T. L. Rhodes, B. W. Rice, S. A. Sabbagh, D. P. Schissel, J. T. Scoville, R. T. Snider, G. M. Staebler, B.

W. Stallard, R. D. Stambaugh, H. E. St. John, R. E. Stockdale, P. L. Taylor, D. M. Thomas, A. D. Turnbull, M. R. Wade, R. Wood, and D. Whyte, Phys. Rev. Lett. **77**, 2714 (1996).
[4]J. A. Wesson, Nucl. Fusion **18**, 87 (1978).
[5]E. A. Lazarus, J. B. Lister, and G. H. Neilson, Nucl. Fusion **30**, 111 (1990).
[6]J. P. Freidberg and F. Haas, Phys. Fluids **16**, 1909 (1973).
[7]J. P. Goedbloed, Phys. Fluids **25**, 2073 (1982).
[8]R. C. Grimm, J. M. Greene, and J. L. Johnson, *Methods in Computational Physics* (Academic, New York, 1976), Vol. 16, p. 253.
[9]L. C. Bernard, F. J. Helton, and R. W. Moore, Comput. Phys. Commun. **24**, 377 (1981).
[10]A. H. Glasser and M. S. Chance, Bull. Am. Phys. Soc. **42**, 1848 (1997).
[11]Y. Q. Liu, A. Bondeson, C. M. Fransson, B. Lennartson, and C. Breitholtz, Phys. Plasmas **7**, 3681 (2000).
[12]J. Bialek, A. H. Boozer, M. E. Mauel, and G. A. Navratil, Phys. Plasmas **8**, 2170 (2001).
[13]R. Fitzpatrick, Phys. Plasmas **9**, 3459 (2002).
[14]H. Jhang, Phys. Plasmas **15**, 022501 (2008).
[15]J. P. Freidberg and F. Haas, Phys. Fluids **17**, 440 (1974).
[16]J. P. Freidberg, *Ideal Magnetohydrodynamics* (Springer, New York, 1987).
[17]D. Pfirsch and H. Tasso, Nucl. Fusion **11**, 259 (1971).